Human Molecular Genetics, 2017, Vol. 26, No. 19 3837–3849

doi: 10.1093/hmg/ddx277
Advance Access Publication Date: 19 July 2017
Original Article

ORIGINAL ARTICLE

Abnormal polyamine metabolism is unique to the neuropathic forms of MPS: potential for biomarker development and insight into pathogenesis

Christian Hinderer[1,†], Nathan Katz[1,†], Jean-Pierre Louboutin[2], Peter Bell[1], Jakub Tolar[3], Paul J. Orchard[3], Troy C. Lund[3], Mohamad Nayal[1], Liwei Weng[4], Clementina Mesaros[4], Carolina F.M. de Souza[5], Amauri Dalla Corte[5,7], Roberto Giugliani[6,7] and James M. Wilson[1,*]

[1]Gene Therapy Program, Department of Medicine, University of Pennsylvania, Philadelphia, PA 19104, USA, [2]Section of Anatomy, Department of Basic Medical Sciences, University of the West Indies, Kingston, Jamaica, [3]Division of Blood and Marrow Transplantation, Department of Pediatrics, University of Minnesota Medical School, Minneapolis, MN 55455, USA, [4]Department of Pharmacology, University of Pennsylvania, Philadelphia, PA 19104, USA, [5]Hospital de Clínicas de Porto Alegre, Rua Ramiro Barcelos, RS Porto Alegre 90035-903, Brazil, [6]Medical Genetics Service, HCPA and [7]Post-Graduate Course in Medical Sciences, UFRGS, Porto Alegre, RS 90035-003, Brazil

*To whom correspondence should be addressed at: Gene Therapy Program, Perelman School of Medicine, University of Pennsylvania, 125 South 31st Street, Suite 1200, Philadelphia, PA 19104, USA. Tel: 215 5739020; Fax: 215 4945444; Email: wilsonjm@upenn.edu

Downloaded from https://academic.oup.com/hmg/article/26/19/3837/3979365 by guest on 21 August 2022

Abstract

The mucopolysaccharidoses (MPS) are rare genetic disorders marked by severe somatic and neurological symptoms. Development of treatments for the neurological manifestations of MPS has been hindered by the lack of objective measures of central nervous system disease burden. Identification of biomarkers for central nervous system disease in MPS patients would facilitate the evaluation of new agents in clinical trials. High throughput metabolite screening of cerebrospinal fluid (CSF) samples from a canine model of MPS I revealed a marked elevation of the polyamine, spermine, in affected animals, and gene therapy studies demonstrated that reduction of CSF spermine reflects correction of brain lesions in these animals. In humans, CSF spermine was elevated in neuropathic subtypes of MPS (MPS I, II, IIIA, IIIB), but not in subtypes in which cognitive function is preserved (MPS IVA, VI). In MPS I patients, elevated CSF spermine was restricted to patients with genotypes associated with CNS disease and was reduced following hematopoietic stem cell transplantation, which is the only therapy currently capable of improving cognitive outcomes. Additional studies in cultured neurons from MPS I mice showed that elevated spermine was essential for the abnormal neurite overgrowth exhibited by MPS neurons. These findings offer new insights into the pathogenesis of CNS disease in MPS patients, and support the use of spermine as a new biomarker to facilitate the development of next generation therapeutics for MPS.

[†]These authors contributed equally to the manuscript.

Received: May 30, 2017. **Revised:** June 29, 2017. **Accepted:** July 11, 2017

© The Author 2017. Published by Oxford University Press. All rights reserved. For Permissions, please email: journals.permissions@oup.com

Introduction

Development of novel therapeutics for rare diseases faces many challenges, including the difficulty of assessing efficacy in clinical trials for which enrollment is limited by small patient populations, phenotypes are heterogeneous, and insufficient natural history data are available to define reliable clinical endpoints. Well-characterized biomarkers can play a critical role in this process by providing rapid objective evidence for the correction of underlying disease pathophysiology, which may in turn predict clinical benefit. Biomarkers can also directly link clinical data to outcomes in preclinical animal studies, and provide a basis for comparison to other established or experimental therapies.

The present study was designed to identify biomarkers useful for evaluating the response to therapies targeting the central nervous system manifestations of mucopolysaccharidosis type I (MPS I). MPS I is a rare recessive disorder caused by mutations in the gene encoding α-L-iduronidase (IDUA), a lysosomal enzyme responsible for the breakdown of complex polysaccharides called glycosaminoglycans (GAGs). MPS I is characterized by systemic accumulation of two GAGs— heparan and dermatan sulfate—that are normally degraded by IDUA. MPS I patients present with a constellation of clinical findings, many of which are directly linked to the mechanical consequences of GAG storage, such as cardiac valve thickening, liver and spleen enlargement, corneal clouding, and airway infiltration (1). Patients with the severe form of MPS I (MPS IH, Hurler syndrome) also exhibit progressive cognitive impairment in early childhood. Intravenous enzyme replacement therapy has proven effective for treating many of the somatic symptoms of MPS I, but the enzyme likely does not cross the blood-brain barrier and has no impact on cognitive outcomes (2–4). Hematopoietic stem cell transplantation (HSCT) performed in the first 2 years of life can attenuate cognitive decline by allowing bone marrow-derived precursors to differentiate into brain macrophages, which serve as a depot of secreted IDUA in the CNS (5–11). However, HSCT is associated with substantial morbidity and mortality and does not fully rescue cognitive function, leaving an unmet need for a safer and more effective CNS-targeted therapy for MPS I.

In this study, we applied high throughput metabolite screening of CSF samples from an animal model of MPS I to identify potential biomarkers of CNS disease, which we then evaluated in MPS patients.

Results

Identification of elevated CSF spermine through metabolite profiling

An initial screen of CSF metabolites was carried out using a canine model of MPS I. These animals have a splice site mutation in the *IDUA* gene, resulting in complete loss of enzyme expression and development of biochemical, clinical, and histological features analogous to those of MPS I patients (12,13). CSF samples were collected from 15 normal dogs and 15 MPS I dogs, and evaluated for relative quantities of metabolites by liquid and gas chromatography coupled with tandem mass spectrometry. A total of 281 metabolites were positively identified in CSF samples. Of these, 47 (17%) were significantly elevated in MPS I dogs relative to controls, and 88 (31%) were decreased relative to controls (Supplementary Material, Table S1). Metabolite profiling revealed marked differences in polyamine, sphingolipid, acetylated amino acid, and nucleotide metabolism between MPS I and normal dogs (Fig. 1A). Random forest clustering analysis identified the polyamine, spermine, as the metabolite most strongly differentiating MPS I from control samples (Supplementary Material, Fig. S1). On average, spermine was elevated 30-fold in MPS I dogs, with the exception of one MPS I dog that was under one month of age at the time of sample collection. CSF spermine elevation was similar for both sexes. An isotope dilution LC-MS/MS assay was developed to quantitatively measure spermine in CSF. Samples evaluated from MPS I dogs at one month and one year of age demonstrated a progressive elevation of CSF spermine relative to age-matched normal controls (Fig. 1B). Heparan sulfate has been identified as a receptor for spermine uptake by cells, which suggests that impaired uptake in MPS I could be responsible for elevated spermine in CSF (14–17). Alternatively, the elevation could be explained by increased spermine synthesis; however, there was no evidence of upregulation of transcriptionally regulated enzymes in the spermine synthesis pathway in brain samples from MPS I dogs (Supplementary Material, Fig. S2).

CNS-directed gene therapy corrects brain storage lesions and reduces CSF spermine in large animal models of MPS I

We have previously described experiments evaluating intrathecal adeno-associated virus (AAV)-mediated gene transfer for the treatment of the central nervous system manifestations of MPS I (18–20). In this approach, an AAV vector carrying the *IDUA* gene is injected into the CSF, allowing for transduction of cells throughout the brain and spinal cord. These transduced cells can then serve as a depot for secretion of the enzyme, which is taken up by the surrounding tissue to achieve widespread resolution of storage lesions. Our studies in two large animal models of MPS I—the MPS I dog and MPS I cat—demonstrated that this approach can globally reduce brain storage lesions. Here, we evaluated CSF spermine levels in treated animals to determine whether changes in CSF spermine correlated with correction of brain pathology.

Five MPS I dogs were treated with an intrathecal injection of an adeno-associated virus serotype 9 vector carrying the canine *IDUA* (c*IDUA*) transgene (Fig. 2A). MPS I dogs can develop antibodies to the normal IDUA enzyme, so two of the dogs were pre-treated as neonates with hepatic c*IDUA* gene transfer to induce immunological tolerance to the protein. Both tolerized dogs exhibited complete resolution of brain storage lesions and CSF IDUA activity above normal levels seven months after IT AAV9-cIDUA treatment (Fig. 2B and C). The three non-tolerized dogs exhibited partial resolution of brain storage lesions and varying levels of IDUA expression, with one animal reaching normal levels and the other two exhibiting expression below normal (Fig. 2B and C). CSF spermine reduction was inversely proportional to brain IDUA activity, with a nearly 3-fold reduction relative to untreated animals in the three dogs treated with the IT vector alone, and a 10-fold reduction in the animals tolerized to cIDUA (Fig. 2D).

We further evaluated the relationship between CSF spermine levels and IDUA reconstitution in MPS I dogs treated with a range of vector doses (Fig. 2E). MPS I dogs previously tolerized to human IDUA by neonatal hepatic gene transfer were treated with an intrathecal injection of an AAV9 vector expressing human IDUA at one of 3 doses (10^{10}, 10^{11}, 10^{12} GC/kg, $n = 2$ per dose). CSF IDUA activity, spermine concentration, and brain storage lesions were evaluated 6 months after injection. There

Downloaded from https://academic.oup.com/hmg/article/26/19/3837/3979365 by guest on 21 August 2022

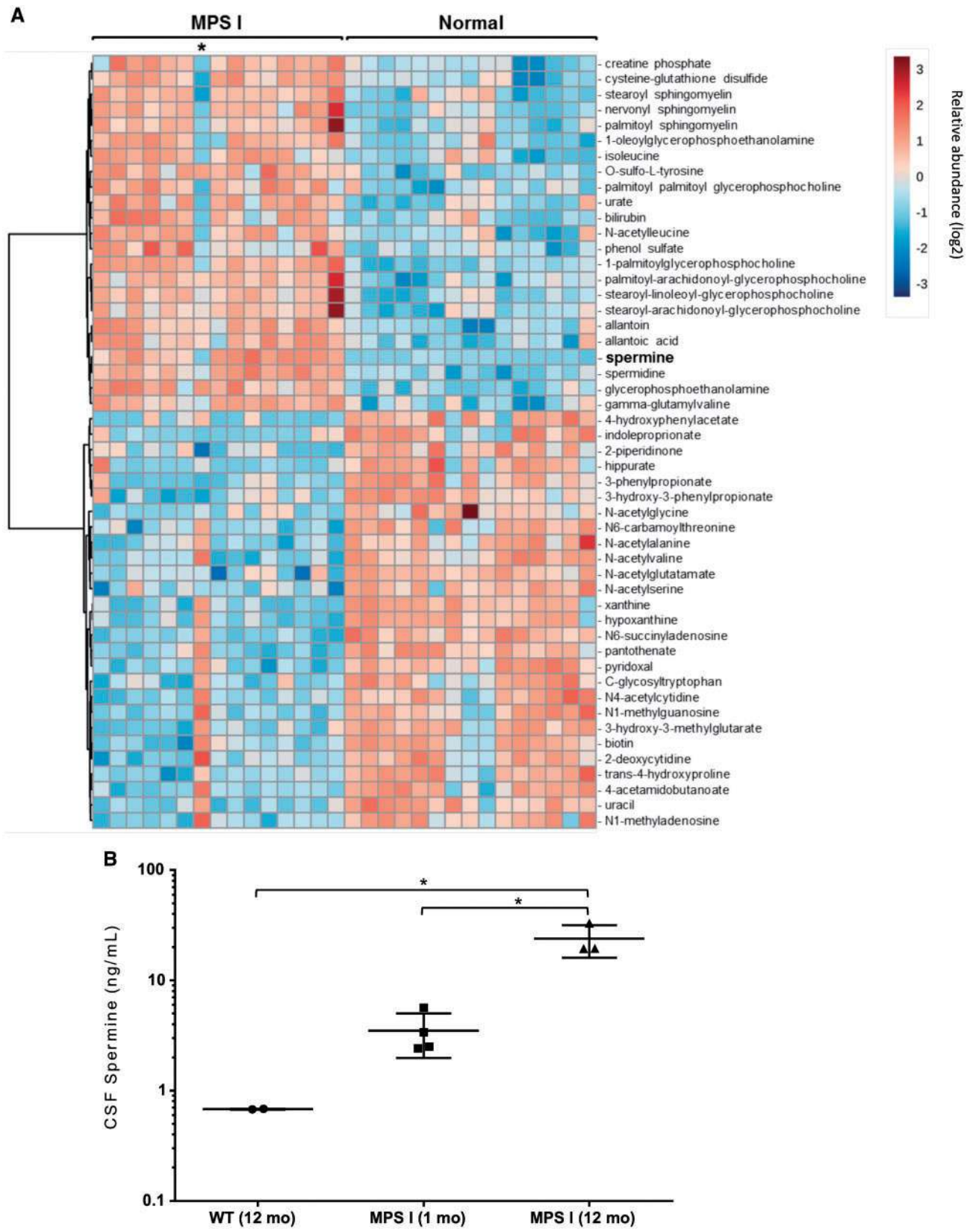

Figure 1. Elevated CSF spermine in MPS I dogs. A high throughput LC-MS/MS and GC-MS/MS metabolite screen was performed on CSF samples from MPS I dogs ($n = 15$) and normal controls ($n = 15$). (**A**) A heatmap of the top 50 differentially detected metabolites (ANOVA) is shown. The youngest animal in the MPS I cohort (28 days of age) is indicated by an asterisk. (**B**) Spermine concentration was measured by a quantitative isotope dilution LC-MS/MS assay in CSF samples from wild type dogs ($n = 2$), one-month-old MPS I dogs ($n = 4$), and one-year-old MPS I dogs ($n = 3$). *$P < 0.05$, one-way ANOVA followed by Tukey's multiple comparisons test.

Downloaded from https://academic.oup.com/hmg/article/26/19/3837/3979365 by guest on 21 August 2022

was dose-dependent expression of IDUA in CSF and correction of brain storage lesions (Fig. 2F and G). Reduction of CSF spermine was dose-dependent, with animals at the mid and high vector doses reaching the normal range, whereas spermine was only partially reduced in the low dose animals (Fig. 2H).

The MPS I cat carries a three base pair in-frame deletion in the *IDUA* gene, resulting in omission of an aspartate residue that renders the enzyme inactive. Like the MPS I dog, these animals develop extensive brain storage lesions. Intrathecal administration of an AAV9 vector expressing feline IDUA partially reconstituted enzyme activity in CSF, cleared brain storage lesions, and normalized CSF spermine levels (Fig. 2I–L).

Elevated CSF spermine in MPS I patients and response to therapy

CSF samples obtained from patients with MPS I ($n = 26$) exhibited significantly elevated spermine levels compared to samples from unaffected children ($n = 21$) (Fig. 3A). Using a threshold of two standard deviations above the mean of control samples (98th percentile), 1/21 control subjects was positive for elevated spermine, whereas 15/26 MPS I patient samples were positive (58%). In twelve MPS I patients, mutations were identified that have been previously correlated with disease severity and CNS involvement (21). In the remaining patients, genotype was either unknown or the genotype-phenotype correlation had not been reported in the literature. Severe mutations universally associated with a severe clinical phenotype and early cognitive decline were present in 8 patients; mutations associated with attenuated disease were present in 4 patients. CSF spermine levels were significantly greater in the patients with severe mutations, with 6/8 (75%) exceeding the 98th percentile of normal, whereas 0/4 patients in the mild mutation cohort met this cutoff (Fig. 3B). MPS I patients classified clinically as having the severe (Hurler) phenotype, which is associated with early developmental delay, had significantly higher CSF spermine levels than patients with the mild (Scheie) form of the disease, in which intellect is preserved (Fig. 3C). Patients with an intermediate Hurler-Scheie phenotype had CSF spermine levels between those of the Hurler and Scheie cohorts. Spermine levels generally appeared to exhibit an inverse correlation with age (Supplementary Material, Fig. S3), though this was likely attributable to ascertainment bias, as all patients greater than 10 years of age for whom samples were available had a diagnosis of Hurler-Scheie or Scheie syndrome. Intravenous enzyme replacement therapy did not impact CSF spermine levels, consistent with the lack of CNS penetration of the enzyme (Supplementary Material, Fig. S4). Hematopoietic stem cell transplantation is currently the only modality capable of attenuating cognitive decline in MPS I patients. One patient, homozygous for a severe *IDUA* mutation, had normal CSF spermine after receiving HSCT (Fig. 3B). Samples from before and after HSCT were available from two MPS I patients with the severe (Hurler) phenotype. Both patients initially had elevated CSF spermine, which declined to the normal range after transplant (Fig. 3E).

Elevated CSF spermine in other neuropathic forms of MPS

Spermine was measured in CSF samples from patients with additional MPS subtypes affecting heparan sulfate metabolism (MPS types II, IIIA, and IIIB) as well as patients with MPS types IVA and VI, which are caused by defects in the metabolism of keratan and dermatan sulfate and do not cause neurocognitive symptoms (22,23). MPS IVA and MPS VI patients had normal CSF spermine levels (Fig. 3A). In contrast, there was marked elevation of CSF spermine in MPS types affecting heparan sulfate catabolism. CSF spermine was significantly greater than normal in samples from MPS II and IIIB patients. Only a single MPS IIIA sample was available, precluding statistical analysis, although this sample fell above the 98th percentile of normal controls. CSF spermine was elevated in MPS II patients classified clinically as having severe or mild disease, though there was no correlation between CSF spermine and disease severity (Fig. 3D). No CSF samples were available from patients with MPS VII, another disorder of heparan sulfate metabolism, though samples from a canine model of MPS VII revealed a marked spermine elevation (Supplementary Material, Fig. S5). These results demonstrate an association between disorders of heparan sulfate metabolism and CSF spermine elevation.

Role of spermine in abnormal neurite growth associated with MPS

It appeared noteworthy that the MPS subtypes affecting heparan sulfate metabolism (MPS I, II, IIIA, IIIB, VII) selectively lead to spermine elevation and are uniquely associated with cognitive dysfunction. Spermine has previously been implicated in neuron growth and development, suggesting that spermine dysregulation could play a direct role in cognitive decline (24–26). Upregulation of polyamine synthesis has been shown to promote neurite outgrowth (24–27), and neurons from a mouse model of MPS IIIB have been shown to exhibit aberrant overgrowth of neurites, potentially leading to defects in neural development and plasticity (28,29). Therefore, we evaluated the role of spermine in the abnormal neurite overgrowth phenotype that has been described in MPS neurons (28). Similar to observations of MPS IIIB neurons, cultured cortical neurons from MPS I mice exhibited greater neurite number, branching, and total arbor length than neurons derived from wild type mice (Fig. 4A and B). Treatment of MPS neurons with APCHA, an inhibitor of spermine synthesis, significantly reduced neurite growth and branching. The effect was reversible by replacing spermine (Fig. 4A and B). The same APCHA concentration did not affect the growth of normal neurons (Supplementary Material, Fig. S6). Addition of spermine to wild type neuron cultures at concentrations similar to those identified *in vivo* resulted in significant increases in neurite growth and branching (Fig. 4A and C).

Growth associated protein 43 (GAP43), a central regulator of neurite growth, is overexpressed by MPS IIIB mouse neurons both *in vitro* and *in vivo*, suggesting that the same neurite growth pathway aberrantly activated in neuron cultures is also active *in vivo* (28–30). GAP43 was measured by Western blot in samples of frontal cortex from MPS I dogs (Fig. 4D and E). GAP43 was upregulated in the cortex of MPS I dogs, and expression was normalized in all gene therapy treated animals.

Discussion

In this study, we set out to identify biomarkers of CNS disease in MPS I using an unbiased metabolite screening approach. The screen revealed substantial disease-related alterations in the CSF metabolome, including a 30-fold elevation in spermine levels compared to normal controls. Spermine appears to be a strong biomarker of CNS disease; it is elevated in the canine and

Downloaded from https://academic.oup.com/hmg/article/26/19/3837/3979365 by guest on 21 August 2022

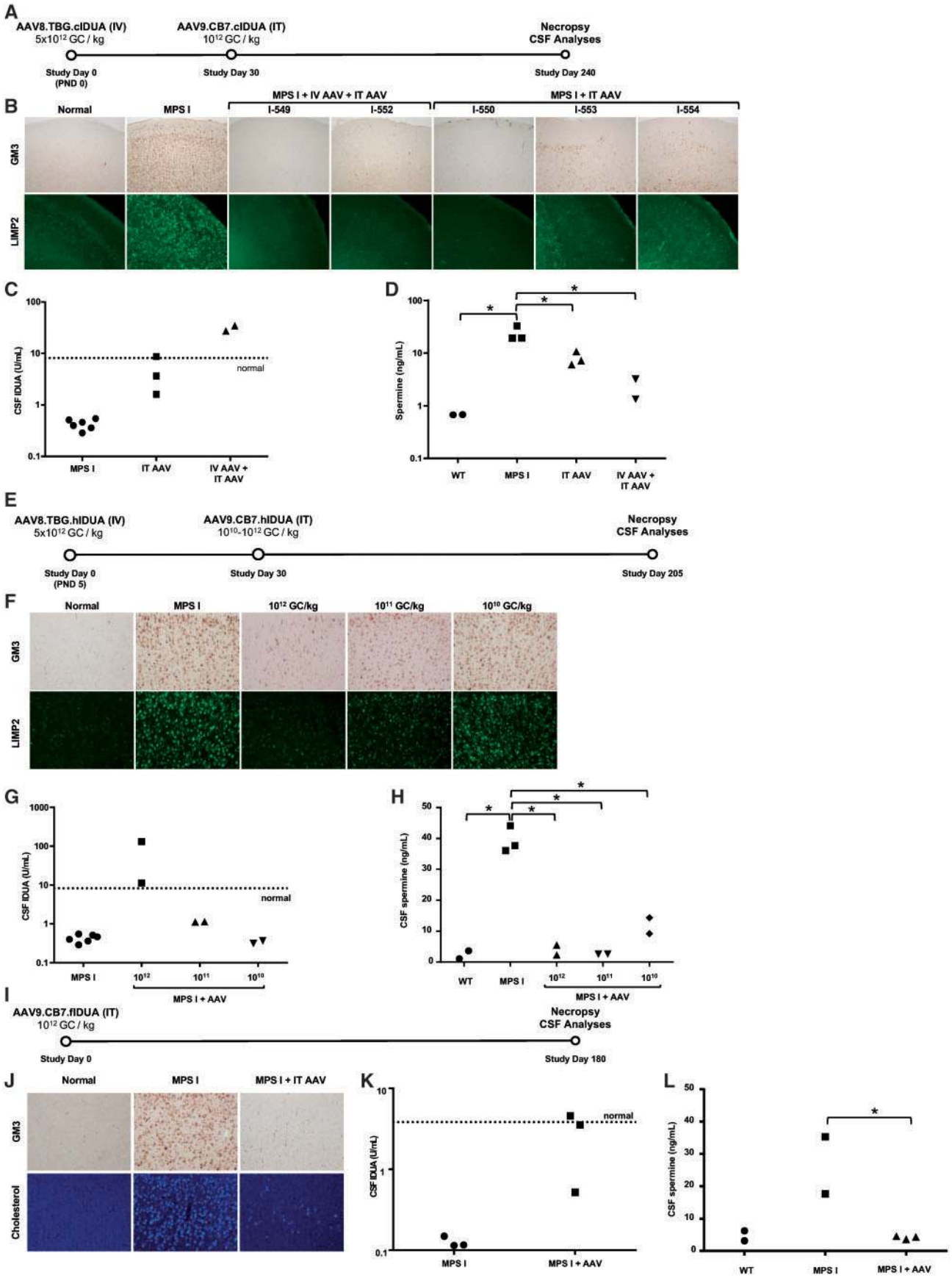

Figure 2. Intrathecal AAV gene therapy corrects brain lesions and normalizes CSF spermine in canine and feline models of MPS I. (A) Experimental design for evaluation of intrathecal AAV9 expressing canine IDUA in MPS I dogs. Animals were treated with an intrathecal injection of AAV9 expressing canine IDUA at one month of age. Two of the animals were pretreated at birth with an IV injection of AAV8 expressing canine IDUA from a liver specific promoter in order to induce tolerance to

Downloaded from https://academic.oup.com/hmg/article/26/19/3837/3979365 by guest on 21 August 2022

feline models of MPS I, and correction of brain lesions by gene therapy directly correlated with reductions in CSF spermine in both models. In MPS I patients, spermine was selectively elevated in those with mutations that cause neurological disease, and was reduced to normal levels by HSCT, a therapy that attenuates cognitive decline (5,6,11). Spermine is also elevated in MPS subtypes associated with neurocognitive manifestations (MPS I, II, IIIA, IIIB), but not those associated only with somatic disease (MPS IVA, VI). Together these findings suggest that spermine correlates with neurological disease in MPS patients, which may make spermine a valuable biomarker for assessing novel therapies designed to treat the CNS lesions associated with neuropathic subtypes of MPS.

Despite the strong correlation between CSF spermine and neuropathic forms of MPS, this pattern did not hold for all patients. Patients with Hurler syndrome, in which neurological disease is universal, exhibited the highest CSF spermine levels of the MPS I patients, but two Hurler patients had CSF spermine levels below the 98th percentile of normal controls. The MPS II patients included in this study had significantly elevated CSF spermine relative to controls, but this elevation was less marked than in MPS I patients and did not correlate with disease severity. It is difficult to interpret the significance of these exceptions in this small study. Subsequent studies with larger cohorts will be needed to fully elucidate the relationship between CSF spermine and central nervous system disease across MPS subtypes, and to evaluate additional factors impacting CSF spermine levels and the variability of CSF spermine measurements for each subject over time. Intriguingly, spermine has been measured *in vivo* using magnetic resonance spectroscopy, raising the possibility of noninvasively evaluating spermine levels in the CNS of MPS patients, which could facilitate larger studies (31).

A CSF biomarker of neurological disease in MPS would have immediate utility for verifying biological activity in first-in-human trials, but may also have an important role in later stage drug development and regulatory approval. For diseases like MPS I, in which there is a small patient population with heterogeneous phenotypes and insufficient natural history data to define rigorous neurocognitive endpoints, the use of well-validated biomarker endpoints can reduce the size, complexity, and duration of clinical trials. To serve as a validated surrogate endpoint, the biomarker must have a clear connection to the pathophysiology of the disease as well as a strong correlation with clinical outcomes. For example, deferiprone was approved by the FDA for iron overload in children with thalassemia based on a reduction in serum ferritin, a biomarker that both mechanistically demonstrates a reduction in iron storage and is predictive of end organ damage (32). Additional studies should evaluate the correlation between CSF spermine normalization and clinical outcomes in patients who have received HSCT. Our preliminary findings indicate that successful HSCT normalizes CSF spermine in patients with MPS IH; if spermine normalization predicts positive cognitive outcomes in a larger cohort, it may be possible to validate this biomarker as a surrogate endpoint, which could significantly facilitate the development of new therapies for the neurocognitive manifestations of MPS.

Beyond its potential as a biomarker, the finding of elevated CSF spermine provides insight into the pathophysiology of MPS. It is perhaps not surprising that spermine is selectively elevated in MPS types associated with defects in heparan sulfate metabolism, given that cellular uptake of spermine is dependent on interactions with heparan sulfate proteoglycans (14,16,17). Cell surface proteoglycans, such as glypican-1, bind spermine through their heparan sulfate moieties, and after endocytosis of the glypican, intracellular cleavage of the heparan chain releases bound spermine into the cell (14,15). Thus, intact heparan sulfate recycling is likely essential for spermine uptake. In MPS, extracellular spermine accumulation could occur through inhibition of this uptake mechanism due to inefficient recycling of the glypican receptor to the Golgi, or abnormal glycosylation resulting from the inability to break down and recycle the component sugars from the lysosome (Fig. 5). Consistent with this model, other ligands for cell surface heparan sulfate proteoglycans, such as fibroblast growth factor, have markedly reduced binding to cells from MPS I patients (33).

It is striking that the MPS subtypes affecting heparan sulfate metabolism (MPS I, II, IIIA, IIIB, and VII), which selectively exhibit spermine accumulation, are also those that manifest with neurocognitive symptoms. A mechanistic link between abnormal heparan sulfate metabolism and cognitive impairment has not yet been established. One explanation for the neurocognitive phenotype of the heparan sulfate storage disorders comes from evidence suggesting that heparan sulfate accumulation leads to abnormal neurite development and overexpression of GAP43, a key protein involved in neurite outgrowth. Murine models of MPS IIIB show regional overexpression of GAP43 in the brain, and cultured neurons from MPS IIIB mice likewise overexpress GAP43 and elaborate longer neurites with more complex branching patterns than normal neurons (28–30). These findings indicate a defect in signaling pathways involved in neuron growth and plasticity, which could explain the development of cognitive dysfunction in MPS patients in the absence of overt neurodegeneration (28,29).

Spermine has been demonstrated to play a role in neurite outgrowth. Following axon injury, there is an upregulation of the rate-limiting enzymes for the synthesis of spermine and its precursors, putrescine and spermidine. This increased polyamine synthesis promotes neurite outgrowth even in the presence of inhibitory signals from myelin (24–27). Further, treatment of neurons with putrescine induces neurite growth when injected directly into CSF, an effect that is blocked by inhibitors of spermine synthesis (25). We found that inhibitors of spermine synthesis blocked excess neurite growth in MPS neurons, and that neurite growth could be induced in WT neurons by spermine concentrations similar to those found in patient CSF. Gene therapy in the dog model of MPS I reversed spermine accumulation and normalized expression of GAP43, suggesting that the same pathway was impacted *in vivo*. The potential for impaired heparan sulfate metabolism to trigger the accumulation of a metabolite that alters neuron growth could point to a novel connection between enzyme deficiencies and abnormal neurite growth in MPS neurons, which may explain the neurocognitive phenotype of these disorders. A mechanistic link between spermine

IDUA. (**B**) Brain storage lesions visualized by staining for GM3 and LIMP2 in WT, MPS I, and AAV9.cIDUA treated dogs. (**C**) CSF IDUA activity at the time of necropsy in untreated and AAV9.cIDUA treated MPS I dogs. (**D**) CSF spermine at the time of necropsy in WT, MPS I, and AAV9.cIDUA treated dogs. (**E**) Experimental design for dose-response study of intrathecal AAV9 expressing human IDUA in MPS I dogs. (**F**) Brain storage lesions visualized by staining for GM3 and LIMP2 in WT, MPS I, and AAV9.hIDUA treated dogs. (**G**) CSF IDUA activity at the time of necropsy in untreated and AAV9.hIDUA treated MPS I dogs. (**H**) CSF spermine at the time of necropsy in WT, MPS I, and AAV9.hIDUA treated dogs. (**I**) Experimental design for evaluation of intrathecal AAV9 expressing feline IDUA in MPS I cats. (**J**) Brain storage lesions visualized by staining for GM3 and unesterified cholesterol in WT, MPS I, and AAV9.fIDUA treated cats. (**K**) CSF IDUA activity at the time of necropsy in untreated and AAV9.fIDUA treated MPS I cats. (**L**) CSF spermine at the time of necropsy in WT, MPS I, and AAV9.fIDUA treated cats. *$P < 0.05$, one-way ANOVA followed by Tukey's multiple comparisons test.

Downloaded from https://academic.oup.com/hmg/article/26/19/3837/3979365 by guest on 21 August 2022

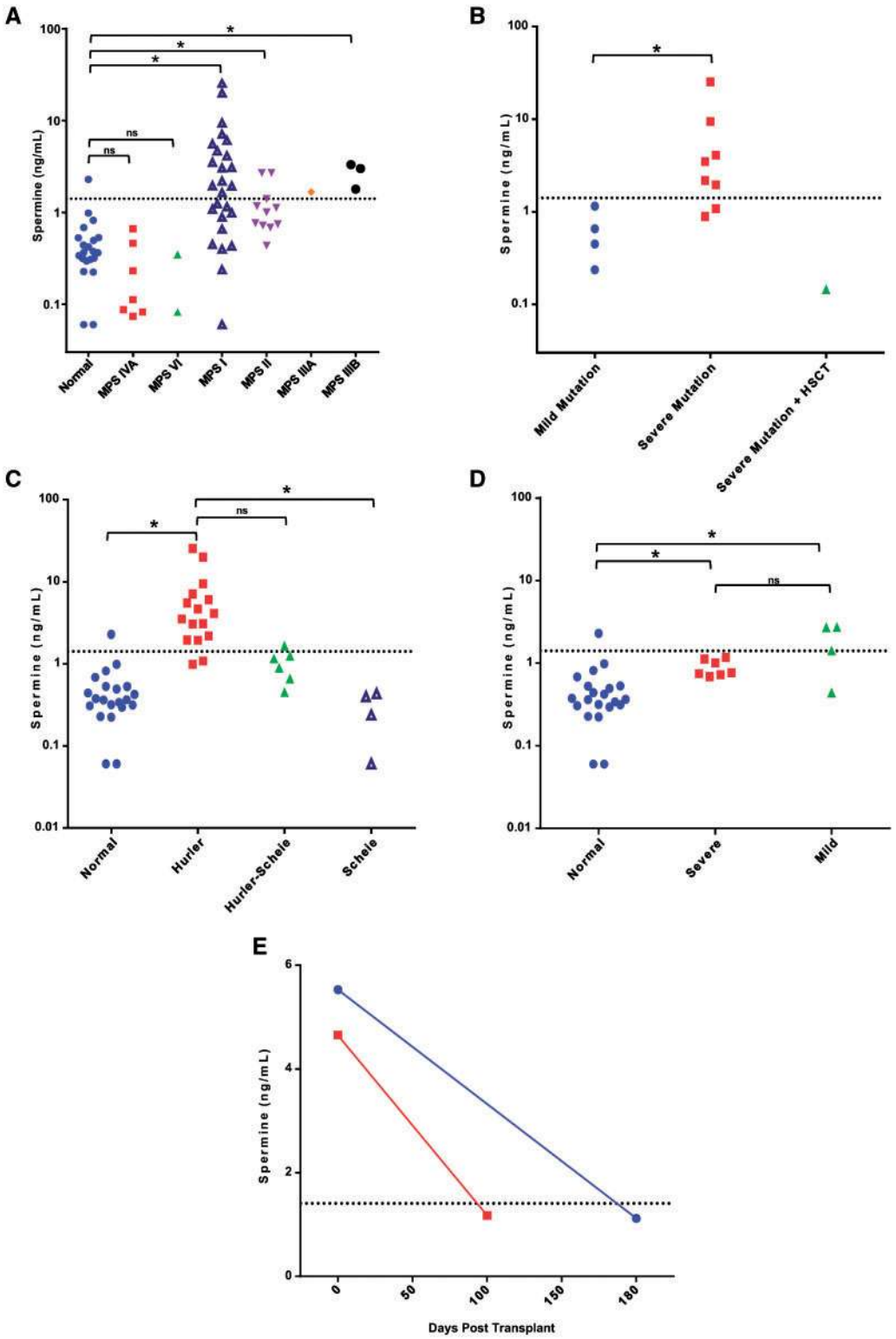

Figure 3. Elevated CSF spermine in MPS patients and response to therapy. (**A**) CSF spermine in patients with MPS IVA ($n = 7$), MPS VI ($n = 2$), MPS I ($n = 26$), MPS II ($n = 11$), MPS IIIA ($n = 1$), MPS IIIB ($n = 3$), and normal controls ($n = 21$). *$P < 0.05$, Kruskal-Wallis test followed by Dunn's multiple comparisons test. (**B**) CSF spermine in MPS I patients with characterized IDUA mutations associated with a mild or severe phenotype. One patient homozygous for a severe mutation (W402X/W402X) previously received a hematopoietic stem cell transplant (green marker). *$P < 0.05$, Mann-Whitney test. (**C**) CSF spermine in MPS I patients based on clinical classification as Hurler, Hurler-Scheie, or Scheie syndrome. *$P < 0.05$, Kruskal-Wallis test followed by Dunn's multiple comparisons test. (**D**) CSF spermine in MPS II patients based on clinical classification as severe or mild phenotype. *$P < 0.05$, Kruskal-Wallis test followed by Dunn's multiple comparisons test. (**E**) CSF spermine in two MPS I patients before and after HSCT. The dotted line indicates the mean + 2SD of spermine concentration in control CSF samples (98th percentile of normal).

Downloaded from https://academic.oup.com/hmg/article/26/19/3837/3979365 by guest on 21 August 2022

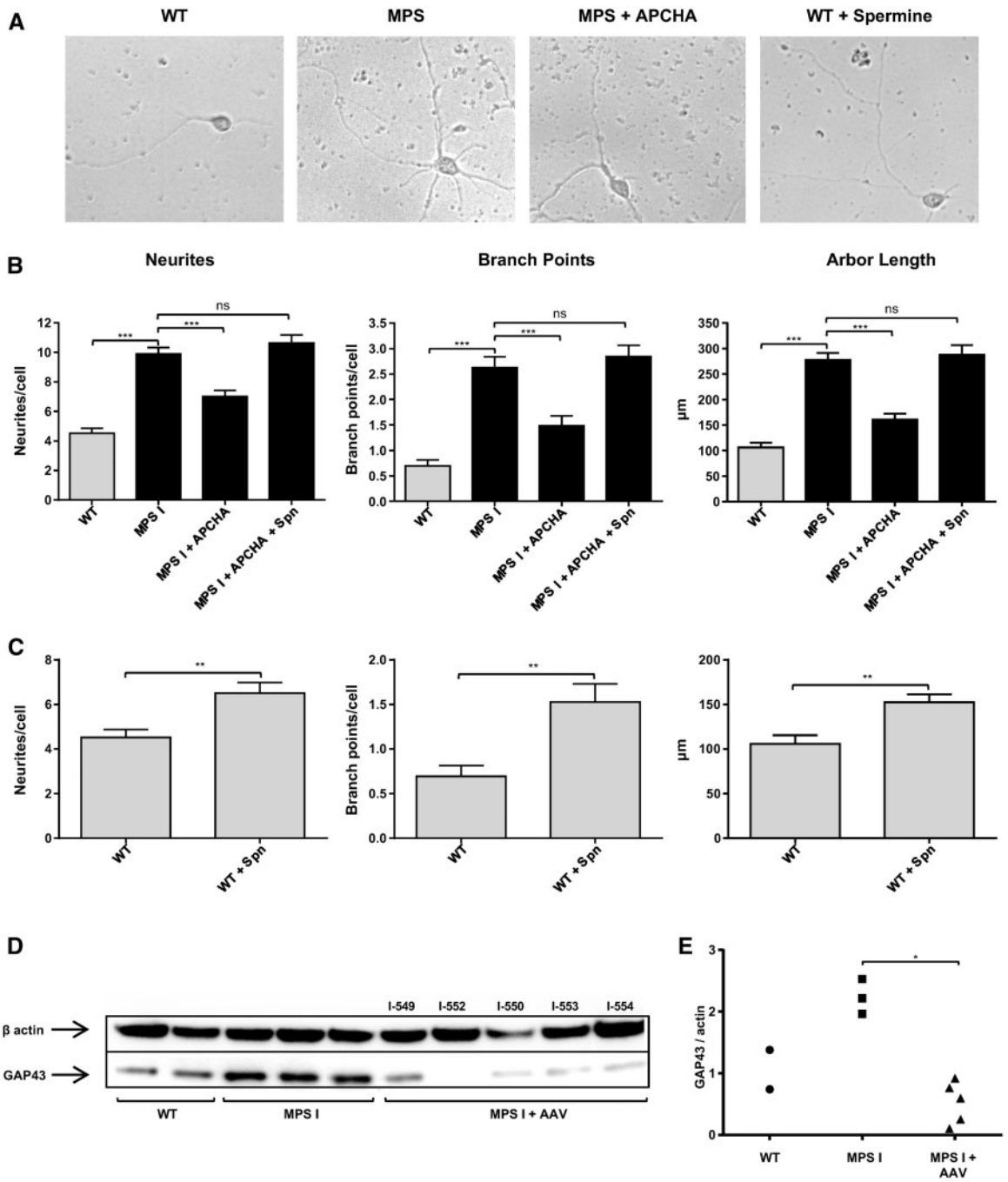

Figure 4. Spermine-dependent aberrant neurite growth in MPS I neurons. Cortical neurons harvested from E18 wild-type or MPS I mouse embryos were treated with spermine or the spermine synthase inhibitor, APCHA, 24 h after plating. (**A**) Phase contrast images were acquired 96 h after plating. (**B**,**C**) Neurite number, length, and branching were quantified for 45-65 randomly selected neurons from duplicate cultures per treatment condition by a blinded reviewer. ***$P < 0.0001$ (ANOVA followed by Dunnett's test), **$P \leq 0.001$ (two-tailed T test). The neurite growth regulating protein, GAP43, was measured in cortical brain samples of untreated MPS I dogs and dogs treated with intrathecal AAV9 by (**D**) Western blot and (**E**) quantified relative to β-actin by densitometry. *$P < 0.05$ (Kruskal-Wallis test followed by Dunn's test).

accumulation and cognitive outcomes would make this a particularly important biomarker for assessment of novel therapies.

Materials and Methods

Patient samples

CSF collection from MPS patients was performed under protocols approved by the Institutional Review Boards of the University of Minnesota (USA) and Hospital de Clínicas de Porto Alegre (Brazil). Samples were collected by lumbar puncture and stored at -80 °C. Samples were de-identified and analyzed in a blinded fashion. Pediatric control CSF samples were obtained from Discovery Life Sciences (Los Osos, CA, USA). As clinical data were not available for these samples, qPCR-based measurement of total DNA was used to identify samples with increased cellularity, which may impact metabolite analysis. Sybr Green PCR was performed using primers targeting the genomic

Downloaded from https://academic.oup.com/hmg/article/26/19/3837/3979365 by guest on 21 August 2022

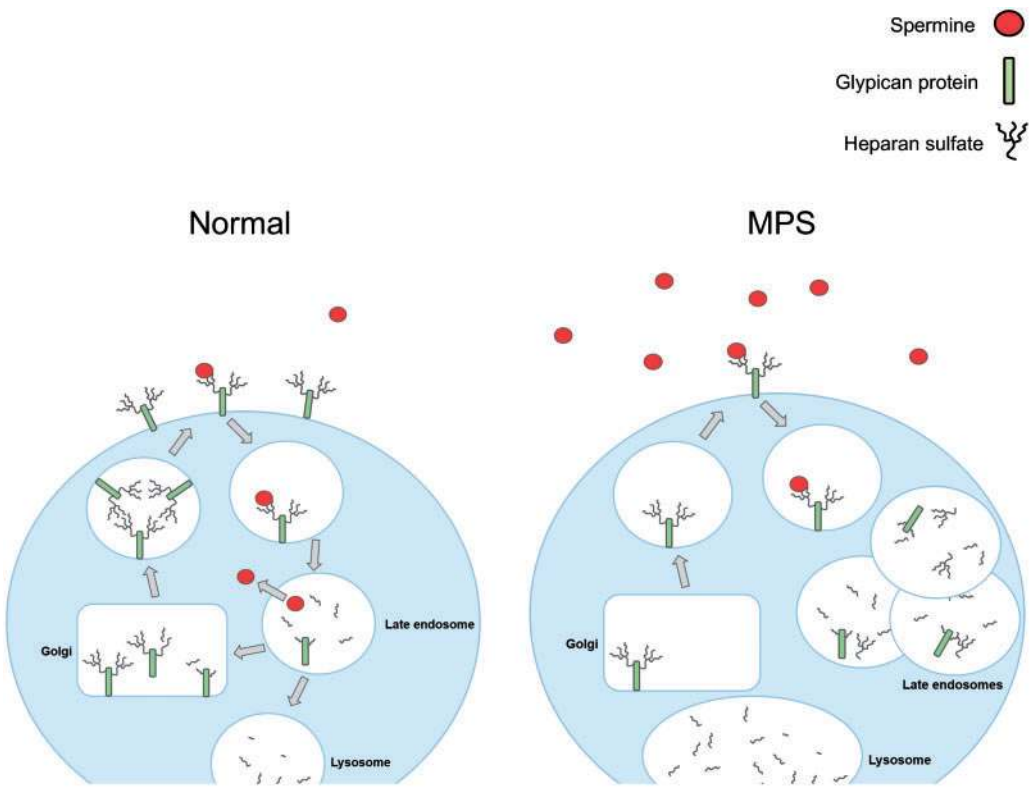

Figure 5. Model of heparan sulfate-dependent spermine uptake. Spermine has been shown to bind to heparan sulfate chains of glypican-1, and spermine uptake can be blocked by both anti-heparan antibodies and enzymatic removal of cell surface heparan sulfate (14–17). After endocytosis of the proteoglycan-spermine complex, the heparan sulfate chain is cleaved from glypican-1, freeing bound spermine (15). The glypican protein core is recycled through the Golgi, where new heparan sulfate chains are added (14,15,39,40). In cells of MPS types associated with impaired heparan sulfate metabolism (MPS I, II, III, VII), there is intracellular accumulation of heparan fragments and heparan-containing proteoglycans, decreased endosomal and Golgi transport, and defects in the surface expression of heparan-modified receptors (33,41,42). Decreased surface presentation and recycling of the receptor in MPS cells may lead to impaired spermine uptake and aberrant accumulation in the extracellular fluid.

GAPDH sequence. Samples with greater than 10x the assay limit of quantification (8/29 samples) were excluded from subsequent analyses. The mean ± SD age for each patient cohort was: MPS I (8 ± 9 years), MPS II (10 ± 8 years), MPS IIIA (8 years), MPS IIIB (8 ± 5 years), MPS IVA (17 ± 12 years), MPS VI (16 ± 1 years), Control (10 ± 6 years). For MPS I patients, *IDUA* mutations classified as severe were W402X, Q70X, and G208D; mutations associated with attenuated CNS disease were R89Q, P533R, and R383H (21).

CSF metabolite profiling

CSF metabolite profiling was performed by Metabolon (Morrisville, NC, USA). Samples were stored at -80 °C until processing. Samples were prepared using the MicroLab STAR® system (Hamilton Company, Reno, NV, USA). A recovery standard was added prior to the first step in the extraction process for QC purposes. Proteins were precipitated with methanol under vigorous shaking for 2 min followed by centrifugation. The resulting extract was divided into five fractions: one for analysis by reverse phase (RP)UPLC-MS/MS with positive ion mode electrospray ionization, one for analysis by RP/UPLC-MS/MS with negative ion mode electrospray ionization, one for analysis by hydrophilic interaction chromatography (HILIC)/UPLC-MS/MS with negative ion mode electrospray ionization, one for analysis by GC-MS, and one sample was reserved for backup. Samples were placed briefly on a TurboVap® (Zymark [now Sotax], Aesch, Switzerland) to remove the organic solvent. For LC, the samples were stored overnight under nitrogen before preparation for analysis. For GC, each sample was dried under vacuum overnight before preparation for analysis.

The LC/MS portion of the platform was based on an ACQUITY ultra-performance liquid chromatography (UPLC) system (Waters Corporation, Milford, MA, USA) and a Q-Exactive high resolution/accurate mass spectrometer interfaced with a heated electrospray ionization (HESI-II) source and Orbitrap mass analyzer operated at 35,000 mass resolution (Thermo Fisher Scientific, Waltham, MA, USA). The sample extract was dried then reconstituted in solvents compatible to each of the LC/MS methods. Each reconstitution solvent contained a series of standards at fixed concentrations to ensure injection and chromatographic consistency. For RP chromatography, one aliquot was analyzed using acidic positive ion optimized conditions and the other using basic negative ion optimized conditions. Each method utilized separate dedicated columns (Waters UPLC BEH C18-2.1 × 100 mm, 1.7 μm). The extracts reconstituted in acidic conditions were gradient eluted using water and methanol containing 0.1% formic acid. The basic extracts were similarly eluted using methanol and water, however, with 6.5 mM ammonium bicarbonate. The third aliquot was analyzed via negative ionization following elution from a HILIC column (Waters UPLC BEH Amide 2.1 × 150 mm, 1.7 μm) using a gradient consisting of water and acetonitrile with

Downloaded from https://academic.oup.com/hmg/article/26/19/3837/3979365 by guest on 21 August 2022

10 mM ammonium formate. The MS analysis alternated between MS and data-dependent MS^n scans using dynamic exclusion. The scan range varied slightly between methods but covered 80-1000 m/z. The samples destined for analysis by GC-MS were dried under vacuum for a minimum of 18 h prior to being derivatized under dried nitrogen using bistrimethylsilyltrifluoroacetamide. Derivatized samples were separated on a 5% diphenyl/95% dimethyl polysiloxane fused silica column (20 m × 0.18 mm ID; 0.18 um film thickness) with helium as carrier gas and a temperature ramp from 60° to 340 °C in a 17.5 min period. Samples were analyzed on a Finnigan Trace DSQ fast-scanning single-quadrupole mass spectrometer (Thermo Fisher Scientific) using electron impact ionization (EI) and operated at unit mass resolving power. The scan range was from 50–750 m/z.

Several types of controls were analyzed in concert with the experimental samples: a pooled matrix sample generated by taking a small volume of each experimental sample served as a technical replicate throughout the data set; extracted water samples served as process blanks; and a cocktail of QC standards that were carefully chosen not to interfere with the measurement of endogenous compounds were spiked into every analyzed sample, which allowed instrument performance monitoring and aided chromatographic alignment. Instrument variability was determined by calculating the median relative standard deviation (RSD) for the standards that were added to each sample prior to injection into the mass spectrometers. Overall process variability was determined by calculating the median RSD for all endogenous metabolites (i.e., non-instrument standards) present in 100% of the pooled matrix samples. Experimental samples were randomized across the platform run, with QC samples spaced evenly among the injections.

Metabolites were identified by automated comparison of the ion features in the experimental samples to a reference library of chemical standard entries that included retention time, molecular weight (m/z), preferred adducts, and in-source fragments as well as associated MS spectra, and curated by visual inspection for quality control using software developed at Metabolon. Identification of known chemical entities was based on comparison to metabolomic library entries of purified standards. Peaks were quantified using area-under-the-curve measurements. Raw area counts for each metabolite in each sample were normalized to correct for variation resulting from instrument inter-day tuning differences by the median value for each run-day, therefore, setting the medians to 1.0 for each run. This preserved variation between samples but allowed metabolites of widely different raw peak areas to be compared on a similar graphical scale. Missing values were imputed with the observed minimum after normalization.

Quantitative MS assay

Quantitative measurements of CSF spermine were performed at the Translational Biomarker Core at the University of Pennsylvania or by Metabolon. For samples processed at the Translational Biomarker Core: CSF samples (50 μl) were mixed with a spermine-d_8 internal standard (IsoSciences, King of Prussia, PA, USA). Samples were deproteinized by mixing with a 4-fold excess of methanol and centrifuging at 12,000 × g at 4 °C. The supernatant was dried under a stream of nitrogen, and then resuspended in 50 μl of water. An aliquot of 5 μl was subjected to LC-MS analysis. The LC separations were carried out using a Waters ACQUITY UPLC system equipped with an Xbridge® C18 column (3.5 μm, 150 × 2.1 mm). The flow-rate was 0.15 mL/min, solvent A was 0.1% formic acid and solvent B was 98/2 acetonitrile/H_2O (v/v) with 0.1% formic acid. The elution conditions were as follows: 2% B at 0 min, 2% B at 2 min, 60% B at 5 min, 80% B at 10 min, 98% B at 11 min, 98% B at 16 min, 2% B at 17 min, 2% B at 22 min, with the column temperature being 35 °C. A Finnigan TSQ Quantum Ultra spectrometer (Thermo Fisher Scientific) was used to conduct MS/MS analysis in positive ion mode with the following parameters: spray voltage at 4000 V, capillary temperature at 270 °C, sheath gas pressure at 35 arbitrary units, ion sweep gas pressure at 2 arbitrary units, auxiliary gas pressure at 10 arbitrary units, vaporizer temperature at 200 °C, tube lens offset at 50, capillary offset at 35, and skimmer offset at 0. The following transitions were monitored: 203.1/112.1 (spermine); 211.1/120.1 (spermine-d_8) with scan width of 0.002 m/z, and scan time being 0.15 s. For samples processed at Metabolon, CSF was spiked with internal standard (spermine-d_8) and subjected to protein precipitation. Following centrifugation, the supernatant was evaporated and reconstituted. An aliquot was injected onto an Agilent (Santa Clara, CA, USA) 1290/AB Sciex QTrap 5500 mass spectrometer LC-MS/MS system equipped with a Waters Acquity BEH C18 column. The peak area of the 203 -> 112 spermine production was measured against the peak area of the respective 211 -> 120 spermine-d_8 internal standard production. Quantitation was performed using a weighted (1/x) linear least squares regression analysis generated from fortified calibration standards prepared immediately prior to each run. The lower limit of quantification was 0.06 ng/ml. Precision and accuracy of the LLOQ was verified by analyzing six samples at the lowest standard concentration in each of the three validation runs.

Animal procedures

All animal protocols were approved by the Institutional Animal Care and Use Committee of the University of Pennsylvania. For CSF metabolite screening, samples were collected by suboccipital puncture in normal dogs at 3–26 months of age, and in MPS I dogs at 1–18 months of age. Gene transfer studies in MPS I dogs and cats were performed as previously described (19,34). CSF samples were collected 6-8 months after vector administration. For mouse cortical neuron experiments, primary cortical neuron cultures were prepared from E18 $IDUA^{-/-}$ or $IDUA^{+/+}$ embryos.

GAP43 Western

Samples of dog frontal cortex were homogenized in 0.2% triton X-100 using a Qiagen (Hilden, Germany) Tissuelyser at 30 Hz for 5 min. Samples were clarified by centrifugation at 4 °C. Protein concentration was determined in supernatants by BCA assay. Samples were incubated in NuPAGE LDS buffer with DTT (Thermo Fisher Scientific) at 70 °C for 1 h and separated on a Bis-Tris 4–12% polyacrylamide gel in MOPS buffer. Protein was transferred to a PVDF membrane and blocked for 1 h in 5% nonfat dry milk. The membrane was probed with rabbit polyclonal anti-GAP43 antibody (Abcam, Cambridge, UK) diluted to 1 μg/ml in 5% nonfat dry milk followed by an HRP conjugated polyclonal anti-rabbit antibody (Thermo Fisher Scientific) diluted 1:10,000 in 5% nonfat dry milk. Bands were detected using SuperSignal West Pico substrate (Thermo Fisher Scientific). Densitometry was performed using Image Lab 5.1 (Bio-Rad Laboratories, Hercules, CA, USA).

Downloaded from https://academic.oup.com/hmg/article/26/19/3837/3979365 by guest on 21 August 2022

Neurite growth assay

Day 18 embryonic cortical neurons were harvested as described above, and plated at a concentration of 100,000 cells/ml on chamber slides (Sigma-Aldrich, St. Louis, MO, USA; S6815) or poly-L-lysine (Sigma-Aldrich) coated tissue culture plates in serum-free Gibco Neurobasal medium (Thermo Fisher Scientific) supplemented by Gibco B27 (Thermo Fisher Scientific). Treatments were applied to duplicate wells 24 h after plating (day 1). Phase-contrast images for quantification were taken on a Nikon Eclipse Ti at 20X using a 600 ms manual exposure and 1.70x gain on high contrast. An individual blind to treatment conditions captured 10–20 images per well and coded them. Images were converted to 8-bit format in ImageJ (34) and traced in NeuronJ (35) by a blinded reviewer. Soma diameter, neurite number, branch points, and arbor length were traced manually. Images traced in NeuronJ were converted to micrometers using a conversion factor based on image size: 2560 x 1920 pixel images were converted to micrometers using a conversion factor of 0.17 micrometers/pixel.

Histology

Brain tissue processing and LIMP2, filipin, and GM3 staining were performed as previously described (18).

RT-PCR

Samples of frontal cortex from 3 normal dogs and 5 MPS dogs were immediately frozen on dry ice at necropsy. RNA was extracted with TRIzol reagent (Thermo Fisher Scientific), treated with DNAse I (Roche, Basel, Switzerland) for 20 min at room temperature, and purified using an RNeasy kit (Qiagen) according to the manufacturer's instructions. Purified RNA (500 ng) was reverse transcribed using the High Capacity cDNA Synthesis Kit (Applied Biosystems, Foster City, CA, USA) with random hexamer primers. Transcripts for arginase, ornithine decarboxylase, spermine synthase, spermidine synthase, spermine-spermidine acetyltransferase, and glyceraldehyde phosphate dehydrogenase were quantified by Sybr green PCR using an Applied Biosystems 7500 Real-Time PCR System. A standard curve was generated for each target gene using 4-fold dilutions of a pooled standard comprised of all individual samples. The highest standard was assigned an arbitrary transcript number, and Ct values for individual samples were converted to transcript numbers based on the standard curve. Values are expressed relative to the *GAPDH* control.

Statistics

The random forest analysis and heat map generation were performed using MetaboAnalyst 3.0 (36–38). Raw peak data were normalized to the mean of normal sample values and log transformed. All other statistical analyses were performed with GraphPad Prism 6 (GraphPad Software, La Jolla, CA, USA).

Supplementary Material

Supplementary Material is available at *HMG* online.

Acknowledgements

We would like to acknowledge Margaret Maronski and the Neuron Culture Services Core (Mahoney Institute of Neurological Sciences, Perelman School of Medicine, University of Pennsylvania) for assistance with neuron isolation and culture. We would like to thank Marc A. Dichter (Mahoney Institute of Neurological Sciences, Perelman School of Medicine, University of Pennsylvania) for providing expertise on neuron culture and morphometric studies. We would like to thank Mark Haskins, Patty O'Donnell, and Jessica Bagel for providing canine CSF samples. We would also like to acknowledge the support of the Morphology Core (Gene Therapy Program, Perelman School of Medicine, University of Pennsylvania). We also thank Jennifer Stewart for editorial assistance with this manuscript.

Conflict of Interest statement. J.M. Wilson is an advisor to REGENXBIO, Dimension Therapeutics, and Solid Gene Therapy, and is a founder of, holds equity in, and has a sponsored research agreement with REGENXBIO and Dimension Therapeutics; in addition, he is a consultant to several biopharmaceutical companies and is an inventor on patents licensed to various biopharmaceutical companies.

Funding

This work was supported by the National Institute of Environmental Health Sciences of the National Institutes of Health under award number P30ES013508, and by the Orphan Disease Center at the University of Pennsylvania.

References

1. Neufeld, E.F. and Muenzer, J. (2014) Beaudet, A.L., Vogelstein, B., Kinzler, K.W., Antonarakis, S.E., Ballabio, A., Gibson, K.M. and Mitchell, G. (eds.), In *Online Metabolic and Molecular Bases of Inherited Disease*. The McGraw-Hill Companies, Inc., New York, NY.
2. Clarke, L.A., Wraith, J.E., Beck, M., Kolodny, E.H., Pastores, G.M., Muenzer, J., Rapoport, D.M., Berger, K.I., Sidman, M., Kakkis, E.D. *et al*. (2009) Long-term efficacy and safety of laronidase in the treatment of mucopolysaccharidosis I. *Pediatrics*, **123**, 229–240.
3. Wraith, J.E., Beck, M., Lane, R., van der Ploeg, A., Shapiro, E., Xue, Y., Kakkis, E.D. and Guffon, N. (2007) Enzyme replacement therapy in patients who have mucopolysaccharidosis I and are younger than 5 years: Results of a multinational study of recombinant human alpha-L-iduronidase (Laronidase). *Pediatrics*, **120**, E37–E46.
4. Wraith, J.E., Clarke, L.A., Beck, M., Kolodny, E.H., Pastores, G.M., Muenzer, J., Rapoport, D.M., Berger, K.I., Swiedler, S.J., Kakkis, E.D. *et al*. (2004) Enzyme replacement therapy for mucopolysaccharidosis I: a randomized, double-blinded, placebo-controlled, multinational study of recombinant human α-L-iduronidase (laronidase). *J. Pediatr*., **144**, 581–588.
5. Aldenboven, M., Boelens, F. and de Koning, T.F. (2008) The clinical outcome of Hurler syndrome after stem cell transplantation. *Biol. Blood Marrow Transplant*, **14**, 485–498.
6. Boelens, J.J., Wynn, R.F., O'Meara, A., Veys, P., Bertrand, Y., Souillet, G., Wraith, J.E., Fischer, A., Cavazzana-Calvo, M., Sykora, K.W. *et al*. (2007) Outcomes of hematopoietic stem cell transplantation for Hurler's syndrome in Europe: a risk factor analysis for graft failure. *Bone Marrow Transplant*, **40**, 225–233.
7. Braunlin, E.A., Stauffer, N.R., Peters, C.H., Bass, J.L., Berry, J.M., Hopwood, J.J. and Krivit, W. (2003) Usefulness of bone

Downloaded from https://academic.oup.com/hmg/article/26/19/3837/3979365 by guest on 21 August 2022

marrow transplantation in the Hurler syndrome. *Am. J. Cardiol.*, **92**, 882–886.
8. Moore, D., Connock, M.J., Wraith, E. and Lavery, C. (2008) The prevalence of and survival in Mucopolysaccharidosis I: Hurler, Hurler-Scheie and Scheie syndromes in the UK. *Orphanet J. Rare Dis.*, **3**, doi:10.1186/1750-1172-1183-1124.
9. Souillet, G., Guffon, N., Maire, I., Pujol, M., Taylor, P., Sevin, F., Bleyzac, N., Mulier, C., Durin, A., Kebaili, K. *et al.* (2003) Outcome of 27 patients with Hurler's syndrome transplanted from either related or unrelated haematopoietic stem cell sources. *Bone Marrow Transplant*, **31**, 1105–1117.
10. Staba, S.L., Escolar, M.L., Poe, M., Kim, Y., Martin, P.L., Szabolcs, P., Allison-Thacker, J., Wood, S., Wenger, D.A., Rubinstein, P. *et al.* (2004) Cord-blood transplants from unrelated donors in patients with Hurler's syndrome. *N. Engl. J. Med.*, **350**, 1960–1969.
11. Whitley, C.B., Belani, K.G., Chang, P.N., Summers, C.G., Blazar, B.R., Tsai, M.Y., Latchaw, R.E., Ramsay, N.K.C. and Kersey, J.H. (1993) Long-term outcome of hurler syndrome following bone-marrow transplantation. *Am. J. Med. Genet.*, **46**, 209–218.
12. Menon, K.P., Tieu, P.T. and Neufeld, E.F. (1992) Architecture of the canine IDUA gene and mutation underlying canine mucopolysaccharidosis I. *Genomics*, **14**, 763–768.
13. Shull, R., Helman, R., Spellacy, E., Constantopoulos, G., Munger, R. and Neufeld, E. (1984) Morphologic and biochemical studies of canine mucopolysaccharidosis I. *Am. J. Pathol.*, **114**, 487–495.
14. Ding, K., Sandgren, S., Mani, K., Belting, M. and Fransson, L.A. (2001) Modulations of glypican-1 heparan sulfate structure by inhibition of endogenous polyamine synthesis. Mapping of spermine-binding sites and heparanase, heparin lyase, and nitric oxide/nitrite cleavage sites. *J. Biol. Chem.*, **276**, 46779–46791.
15. Belting, M., Mani, K., Jönsson, M., Cheng, F., Sandgren, S., Jonsson, S., Ding, K., Delcros, J.-G. and Fransson, L.-Å. (2003) Glypican-1 is a vehicle for polyamine uptake in mammalian cells a pivotal role for nitrosothiol-derived nitric oxide. *J. Biol. Chem.*, **278**, 47181–47189.
16. Belting, M., Persson, S. and Fransson, L.-Å. (1999) Proteoglycan involvement in polyamine uptake. *Biochem. J.*, **338**, 317–323.
17. Welch, J.E., Bengtson, P., Svensson, K., Wittrup, A., Jenniskens, G.J., Ten Dam, G.B., Van Kuppevelt, T.H. and Belting, M. (2008) Single chain fragment anti-heparan sulfate antibody targets the polyamine transport system and attenuates polyamine-dependent cell proliferation. *Int. J. Oncol.*, **32**, 749–756.
18. Hinderer, C., Bell, P., Gurda, B.L., Wang, Q., Louboutin, J.-P., Zhu, Y., Bagel, J., O'Donnell, P., Sikora, T., Ruane, T. *et al.* (2014) Intrathecal gene therapy corrects CNS pathology in a feline model of mucopolysaccharidosis I. *Mol. Ther.*, **22**, 2018–2027.
19. Hinderer, C., Bell, P., Louboutin, J.P., Zhu, Y., Yu, H., Lin, G., Choa, R., Gurda, B.L., Bagel, J., O'Donnell, P. *et al.* (2015) Neonatal systemic AAV induces tolerance to CNS gene therapy in MPS I dogs and nonhuman primates. *Mol. Ther.*, **23**, 1298–1307.
20. Hinderer, C., Bell, P., Louboutin, J.-P., Katz, N., Zhu, Y., Lin, G., Choa, R., Bagel, J., O'Donnell, P., Fitzgerald, C.A. *et al.* (2016) Neonatal tolerance induction enables accurate evaluation of gene therapy for MPS I in a canine model. *Mol. Genet. Metab.*, **119**, 124–130.
21. Matte, U., Yogalingam, G., Brooks, D., Leistner, S., Schwartz, I., Lima, L., Norato, D.Y., Brum, J.M., Beesley, C., Winchester, B. *et al.* (2003) Identification and characterization of 13 new mutations in mucopolysaccharidosis type I patients. *Mol. Genet. Metab.*, **78**, 37–43.
22. Vairo, F., Federhen, A., Baldo, G., Riegel, M., Burin, M., Leistner-Segal, S. and Giugliani, R. (2015) Diagnostic and treatment strategies in mucopolysaccharidosis VI. *The Application of Clinical Genetics*, **8**, 245–255.
23. Hendriksz, C.J., Harmatz, P., Beck, M., Jones, S., Wood, T., Lachman, R., Gravance, C.G., Orii, T. and Tomatsu, S. (2013) Review of clinical presentation and diagnosis of mucopolysaccharidosis IVA. *Mol. Genet. Metab.*, **110**, 54–64.
24. Cai, D., Deng, K., Mellado, W., Lee, J., Ratan, R.R. and Filbin, M.T. (2002) Arginase I and polyamines act downstream from cyclic AMP in overcoming inhibition of axonal growth MAG and myelin in vitro. *Neuron*, **35**, 711–719.
25. Deng, K., He, H., Qiu, J., Lorber, B., Bryson, J.B. and Filbin, M.T. (2009) Increased synthesis of spermidine as a result of upregulation of arginase I promotes axonal regeneration in culture and in vivo. *J. Neurosci.*, **29**, 9545–9552.
26. Schreiber, R.C., Boeshore, K.L., Laube, G., Veh, R.W. and Zigmond, R.E. (2004) Polyamines increase in sympathetic neurons and non-neuronal cells after axotomy and enhance neurite outgrowth in nerve growth factor-primed PC12 cells. *Neuroscience*, **128**, 741–749.
27. Gao, Y., Deng, K., Hou, J., Bryson, J.B., Barco, A., Nikulina, E., Spencer, T., Mellado, W., Kandel, E.R. and Filbin, M.T. (2004) Activated CREB is sufficient to overcome inhibitors in myelin and promote spinal axon regeneration in vivo. *Neuron*, **44**, 609–621.
28. Hocquemiller, M., Vitry, S., Bigou, S., Bruyère, J., Ausseil, J. and Heard, J.M. (2010) GAP43 overexpression and enhanced neurite outgrowth in mucopolysaccharidosis type IIIB cortical neuron cultures. *J. Neurosci. Res.*, **88**, 202–213.
29. Vitry, S., Ausseil, J., Hocquemiller, M., Bigou, S., dos Santos Coura, R. and Heard, J.M. (2009) Enhanced degradation of synaptophysin by the proteasome in mucopolysaccharidosis type IIIB. *Mol. Cell. Neurosci.*, **41**, 8–18.
30. Li, H.H., Zhao, H.Z., Neufeld, E.F., Cai, Y. and Gómez-Pinilla, F. (2002) Attenuated plasticity in neurons and astrocytes in the mouse model of Sanfilippo syndrome type B. *J. Neurosci. Res.*, **69**, 30–38.
31. Thomas, M.A., Nagarajan, R., Huda, A., Margolis, D., Sarma, M.K., Sheng, K., Reiter, R.E. and Raman, S.S. (2014) Multidimensional MR spectroscopic imaging of prostate cancer in vivo. *NMR Biomed.*, **27**, 53–66.
32. FDA. (2011) FDA approves Ferriprox to treat patients with excess iron in the body. *Press Release*.
33. Pan, C., Nelson, M.S., Reyes, M., Koodie, L., Brazil, J.J., Stephenson, E.J., Zhao, R.C., Peters, C., Selleck, S.B., Stringer, S.E. *et al.* (2005) Functional abnormalities of heparan sulfate in mucopolysaccharidosis-I are associated with defective biologic activity of FGF-2 on human multipotent progenitor cells. *Blood*, **106**, 1956–1964.
34. Rasband, W.S. (1997). National Institutes of Health, Bethesda, MD, USA.
35. Meijering, E., Jacob, M., Sarria, J.C., Steiner, P., Hirling, H. and Unser, M. (2004) Design and validation of a tool for neurite tracing and analysis in fluorescence microscopy images. *Cytometry A*, **58**, 167–176.
36. Xia, J., Mandal, R., Sinelnikov, I.V., Broadhurst, D. and Wishart, D.S. (2012) MetaboAnalyst 2.0—a comprehensive server for metabolomic data analysis. *Nucleic Acids Res.*, **40**, W127–133.
37. Xia, J., Psychogios, N., Young, N. and Wishart, D.S. (2009) MetaboAnalyst: a web server for metabolomic

Downloaded from https://academic.oup.com/hmg/article/26/19/3837/3979365 by guest on 21 August 2022

data analysis and interpretation. *Nucleic Acids Res*., **37**, W652–W660.
38. Xia, J., Sinelnikov, I.V., Han, B. and Wishart, D.S. (2015) MetaboAnalyst 3.0—making metabolomics more meaningful. *Nucleic Acids Res*., **43**, W251–257.
39. Mani, K., Cheng, F. and Fransson, L.A. (2006) Constitutive and vitamin C-induced, NO-catalyzed release of heparan sulfate from recycling glypican-1 in late endosomes. *Glycobiology*, **16**, 1251–1261.
40. Mani, K., Jönsson, M., Edgren, G., Belting, M. and Fransson, L.-Å. (2000) A novel role for nitric oxide in the endogenous degradation of heparan sulfate during recycling of glypican-1 in vascular endothelial cells. *Glycobiology*, **10**, 577–586.
41. McCarty, D.M., DiRosario, J., Gulaid, K., Killedar, S., Oosterhof, A., van Kuppevelt, T.H., Martin, P.T. and Fu, H. (2011) Differential distribution of heparan sulfate glycoforms and elevated expression of heparan sulfate biosynthetic enzyme genes in the brain of mucopolysaccharidosis IIIB mice. *Metab. Brain Dis*, **26**, 9–19.
42. Lemonnier, T., Blanchard, S., Toli, D., Roy, E., Bigou, S., Froissart, R., Rouvet, I., Vitry, S., Heard, J.M. and Bohl, D. (2011) Modeling neuronal defects associated with a lysosomal disorder using patient-derived induced pluripotent stem cells. *Hum. Mol. Genet*., **20**, 3653–3666.

Downloaded from https://academic.oup.com/hmg/article/26/19/3837/3979365 by guest on 21 August 2022